https://doi.org/10.3311/PPci.43609

Periodica Polytechnica Civil Engineering

Mechanism-based Interpretation of Soil Arching in Piled Embankments Based on Compression–Extension Zoning

Mostafa Almasraf[1], Araz Salimnezhad[1], Bedirhan Enes Kelek[2], Ozer Cinicioglu[2], Safiye Feyza Cinicioglu[1*]

[1] Department of Civil Engineering, Ozyegin University, Cekmekoy, 34794, Istanbul, Turkey
[2] Department of Civil Engineering, Bogazici University, Besiktas, 34342, Istanbul, Turkey
[*] Corresponding author, e-mail: feyza.cinicioglu@ozyegin.edu.tr

Received: 15 December 2025, Accepted: 08 June 2026, Published online: 17 July 2026

Abstract

The behavior and design of piled embankments constructed on soft soils are governed largely by soil arching, defined as the redistribution of stresses from yielding zones to adjacent non-yielding regions resulting from stiffness contrasts between pile-supported and unsupported areas. Lateral spreading also constitutes a significant component of the load redistribution within the embankment. Arching is characterized by the spatial distribution of the lateral earth pressure coefficient (K). K-contours delineate the compression ($K > K_0$) and extension ($K < K_0$) zones, while the K_0 isoline defines the interface between these regions and thereby represents arch geometry. This study employs full-scale finite element modelling to investigate arching development while accounting for lateral spreading in both high- and low embankments. Results show a transition from shear-plane arching at low fill heights to partial and ultimately full arching beyond a critical height, after which further increases in fill height have limited influence on arch geometry. Extraction of K-fields from FEM highlights the governing role of system deformation in stress redistribution. A parametric comparison between FEM and analytical design methods across varying pile spacings and embankment heights reveals stage-dependent arching evolution, characterized by an initial sharp decrease in stress reduction ratio followed by gradual stabilization as embankment height increases. Among the analytical methods, Hewlett and Randolph and BS8006-1 show the closest agreement with FEM trends. The commonly accepted equal settlement plane concept is shown to be valid primarily for closely spaced piles, whereas for wider spacings, differential settlements persist well above the critical embankment height.

Keywords

soil arching, lateral earth pressure coefficient (K), pile-supported embankments, full-scale embankment finite element model, critical embankment height

1 Introduction

The arching mechanism in granular materials was first recognized in the late 19th century during the construction of military magazine silos [1]. Its modern definition, describing the transfer of stress from a yielding zone of soil to adjacent, less yielding zones, was first introduced by Terzaghi at the 1st International Conference on Soil Mechanics and Foundation Engineering [2]. In any project involving neighboring soil bodies that yield differently, engineers need to consider the effects of arching. These include, but are not limited to, embankments, railways, highways, and tunnels [3–12].

The first meaningful insight came from physical modeling. Trapdoor tests showed that as the movable base is lowered, the vertical stress above the door decreases, while the reactions on the adjoining stationary zones increase, indicating stress redistribution. Later two-dimensional and three-dimensional laboratory models, centrifuge experiments at elevated g-levels [6], and full-scale observations have documented how arches form, evolve, and degrade as relative displacement increases [6, 12]. Analytical work has tended to follow three main lines. One treats the problem as an equilibrium of soil blocks inspired by trapdoor or conduit analogies, often in plane strain, to quantify the portion of overburden diverted away from the yielding zone [13]. A second family idealizes three-dimensional transfer by adopting dome or shell forms, sometimes coupled with basal reinforcement, to partition embankment load among piles, geosynthetics, and the intervening

Cite this article as: Almasraf, M., Salimnezhad, A., Kelek, B. E., Cinicioglu, O., Cinicioglu, S. F. "Mechanism-based Interpretation of Soil Arching in Piled Embankments Based on Compression–Extension Zoning", Periodica Polytechnica Civil Engineering, 2026. https://doi.org/10.3311/PPci.43609

subsoil [10, 11]. A third approach represents arch evolution as a staged process and relates an arching ratio to relative displacement through a ground-reaction-type curve [14–16]. Although these models differ in assumed geometry and simplifications, they share a common objective: to connect boundary movement to stress redistribution in a way that remains transparent for design.

Numerical analysis complements both experiment and theory. Continuum analysis, such as finite element and finite difference methods [3, 17], captures staged construction, consolidation, and global stress paths, and they allow the extraction of spatial fields of stress, strain, and pore pressure across the entire model. Discrete element simulations [18, 19] resolve grain-scale interactions and reveal the emergence of force chains that serve as the arch's skeleton; parameters such as interparticle friction, angularity, and contact stiffness govern the robustness of these chains. The two families are therefore best viewed as compatible rather than competing: DEM clarifies micromechanics, while continuum models connect those choices to field-scale response under realistic boundary conditions.

This paper examines the arching mechanism by analyzing spatial variation in the lateral earth pressure coefficient (K) along piled embankments using finite-element analysis. Unlike the conventional unit-cell approaches commonly used to analyze arching problems, the present study considers the full-scale embankment. This full-scale approach permits the evolution of arching and stress redistribution, accounting for lateral spreading of the fill toward the toes. This configuration provides a more realistic and precise representation of in-situ behavior.

The results of the analysis, which consider the variation in the lateral earth pressure coefficient, K, are benchmarked against the at-rest reference K_0 and the familiar active-passive bounds. The applied procedure could easily reveal the geometrical patterns of the arches, given the inherent ability of the K values to separate regions undergoing compression from those undergoing relaxation.

To further explain the mechanisms governing soil arching, the evolution of K isolines was examined throughout staged embankment construction. The results reveal a progressive transition from shear-plane arching at low fill heights to the development of a well-defined full arch as the embankment height increases. The boundary between relaxation and compression zones, identified by $K_0 = 0.5$, provides a clear mechanical interpretation of arch formation and stress redistribution. The proposed visualization approach enables precise identification of arch geometry and its evolution with increasing overburden pressure. To address the variability in predictions among existing design approaches for piled embankments, a systematic parametric study was undertaken. The performance of six commonly used design methods was evaluated against numerical finite element analyses over a range of pile spacings and embankment heights. The comparison focused on the sensitivity of each method to variations in key governing parameters and on its ability to reproduce the stress transfer mechanisms captured numerically. Since these analytical approaches are formulated for the practical three-dimensional applications, the numerical results were interpreted using the three-dimensional stress reduction ratio (S_{3D}), enabling a consistent assessment of soil arching behavior. Using the method proposed in this study, the critical embankment height was determined for each analyzed model. These values were then compared with those obtained from the correlations available in the literature, and the results of the proposed method were found to lie approximately within the range defined by the existing correlations. One additional important consideration in analyzing arching behavior is the equal settlement plane, defined as the level of height above which there is no differential settlement. There is a generally accepted approach to finding an equal settlement plane in the literature, but the application of it in the current study for the widely spaced piles did not exhibit the presence of such an equal settlement plane. Therefore, this paper recommends improving and generalizing the concept to cover cases with wider pile spacings to determine differential settlement at the considered level and refers to it as the "differential settlement prediction plane".

2 Numerical model and material properties

The conventional pile-supported (CPS) embankments under self-weight in plane-strain 2D conditions were modeled using the finite element method (FEM)-based software, Plaxis 2D [20]. The soil profile of Stanstead Abbots (Willow Plantation or Harlow) was selected as a well-documented case history to represent the soft ground over which the embankment will be constructed [21–24]. The Stanstead Abbotts embankment was constructed on very soft alluvial deposits with a height of 8.05 m in 274 days. The soil stratigraphy and the validated geotechnical properties of Stanstead Abbotts are presented in Fig. 1 and Table 1, respectively. The groundwater is located at a depth of 1.5 m beneath the ground surface. The behavior of the soft ground beneath the embankment was modeled

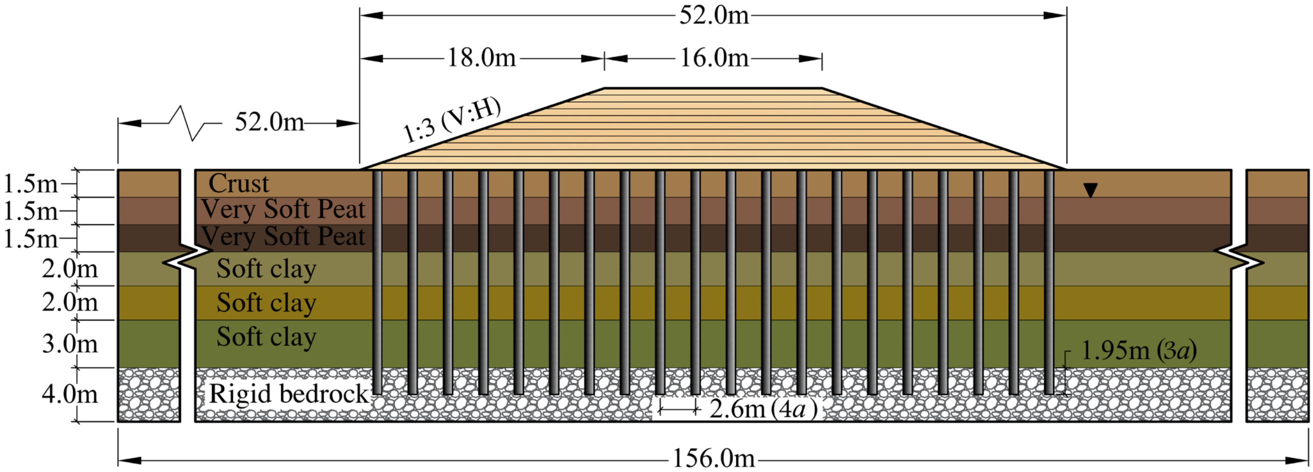

Fig. 1 Considered numerical full-scale embankment model and sub-soil sample

Table 1 Material parameters for the piled embankment

Material	Soil model	Unit weight γ (kN/m^3)	Poisson's ratio v_{ur}	Permeability $k_x = k_y$ (m/s)	Void ratio e_0	Adopted from Hird et al. [24] λ^*	κ^*	ϕ (°)
Crust	Soft soil	16	0.15	2.5×10^{-5}	0.8	0.060	0.009	29
Very soft peat		11.4	0.15	2.5×10^{-5}	7.3	0.147	0.006	34
Very soft peat		11.4	0.15	2.5×10^{-5}	8.2	0.179	0.020	34
Soft clay		16.2	0.15	2.5×10^{-10}	1.5	0.163	0.015	28
Soft clay		16.2	0.15	2.5×10^{-10}	1.45	0.158	0.013	28
Soft clay		16.2	0.15	2.5×10^{-10}	1.4	0.060	0.009	28
Embankment fill	Hardening soil	19	0.2	4×10^{-5}	0.5	E_{50}^{ref} (kN/m^2) 25×10^3	E_{oed}^{ref} (kN/m^2) 25×10^3	E_{ur}^{ref} (kN/m^2) 75×10^3
Bedrock	Mohr-Coulomb	27.5	0.3	-	0.5	E'_{ref} (kN/m^2) 4.9×10^6	-	-
Pile	Linear elastic	24	0.3	-	-	30×10^6	-	-

using the Soft-Soil Model, which incorporates undrained loading stages followed by consolidation stages. Using the subsoil profile of Stanstead Abbots and adding the piles into the system, five different heights (2 m, 4 m, 6 m, 8 m, and 10 m) were considered to analyze the behavior of the CPS piled embankments resting on the considered soil profile.

The staged construction technique was adopted, and layer placement thicknesses were chosen as 0.5 m each. After completion of fill construction, excess pore water pressure was allowed to dissipate during the final consolidation phase.

The angle of interface friction is taken as $2/3\phi'$ by applying a 2/3 reduction factor to the shear strength angle of the soil surrounding the piles. The soil profile ends with a bedrock layer at the bottom. Piles of 13.45 m are embedded to a depth of $3a$ into the bedrock. The pile diameters (a) are taken as 0.65 m across all models. The center-to-center spacing of the piles varied as $4a$, $5a$, and $6a$.

2.1 Soft soil model validation

The Stanstead Abbotts embankment, constructed on very soft alluvial deposits, reached a final height of 8.05 m over a period of 274 days. The staged construction sequence (Fig. 2 [23, 24]) is simulated in the finite element (FE) analysis to accurately replicate the corresponding in-situ loading conditions. The subsurface soil profile was previously modeled by Oztoprak and Cinicioglu [23] using the Soft Soil Creep and Modified Cam Clay models. As the primary aim of the current study was to investigate the mechanism and evolution of arching, a soft soil model was adopted that accounted for the primary consolidation behavior of the soft soil layers. The soft soil model is based on the Cam-Clay model and is particularly well-suited for modeling normally and lightly over-consolidated clays, silty clays, and peat. The stress-strain response of the subsoil during construction loading was numerically derived and compared with reported stress-strain measurements for in

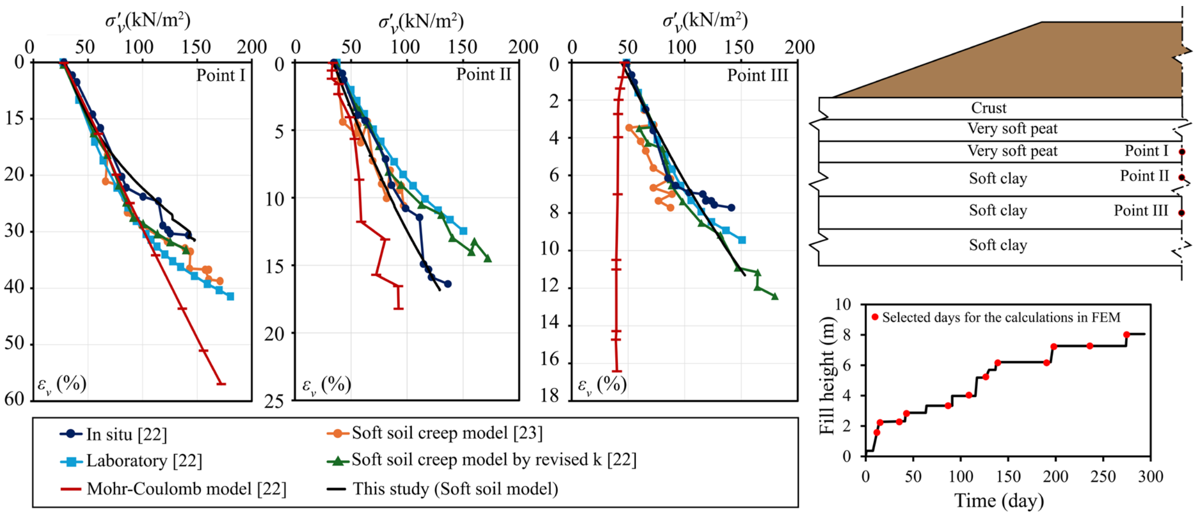

Fig. 2 Soft-Soil Model validation compared to experimental and numerical data

situ, laboratory, and Mohr-Coulomb model [23], as well as the Soft Soil Creep model [24] and the Soft Soil Creep model with a revised permeability coefficient (*k*) [23], for validation purposes. For this comparison, the mid-depths of the second, third, and fourth soil layers (Points I, II, and III, respectively, in Fig. 2 [23, 24]) were selected as reference points to evaluate the soft soil model's accuracy in capturing the stress-strain behavior obtained by other soil models and field/laboratory data.

The validation results are presented in Fig. 2 [23, 24]. The current numerical modeling approach, which incorporates staged construction conditions and employs the Soft Soil model, exhibits satisfactory agreement with the in-situ observations. The stress-strain results obtained using the Soft Soil model in this study also showed good agreement with the other models, as shown in the comparative graph, except for the Mohr-Coulomb model, thereby confirming the model's reliability and providing a basis for the subsequent simulations.

3 A proposed method to find arch geometry

This paper presents a novel method for investigating arching behavior in FEM models of piled embankments on soft soil by analyzing the variation of the lateral earth pressure coefficient (*K*) throughout the embankment. Unlike conventional approaches, using spatial *K*-value contours provides a more precise characterization of arching, particularly in full-scale models with sufficiently distant lateral boundaries. This method enables more reliable identification of soil arch geometry, arch height, and the equal settlement plane, while accounting for lateral deformation.

Most existing studies on arching mechanisms rely on a unit-cell approach, which considers only a limited vertical cross-section of the embankment. This approach may not adequately represent the actual deformation and stress redistribution within the full embankment system. Focusing on a restricted section can also introduce inconsistencies in the treatment of boundary conditions. Therefore, accurate interpretation of arching behavior in CPS embankments using FE analysis requires modeling the entire embankment, as adopted in this study.

Beyond modeling the entire embankment, a representative method is required to interpret the evolution of the arching mechanism. Previous studies have identified soil arch geometry using vertical, horizontal, or principal stresses [3, 21, 22, 25–27], typically along vertical sections between piles. According to these approaches, the first deviation from the geostatic pressure line marks the upper arch boundary, and the point where the stress curve returns toward geostatic pressure marks the lower boundary. Vertical and horizontal stress-based methods can yield inconsistent results and fail to capture realistic arch geometry. These approaches approximate the arch using discrete points obtained from multiple vertical cross-sections between adjacent piles, making the procedure cumbersome and time-consuming (Fig. 3).

Fig. 3(a) presents a comparison of effective lateral stress variations in an 8 m high embankment constructed on soft soil and on a rigid base. The soft-soil case corresponds to a piled embankment with 4*a* pile spacing, while the rigid-base model isolates the fill self-weight effect by eliminating subsoil deformation. The comparison is conducted along the embankment's centerline, at the midpoint between the central piles. In Fig. 3(a), the rigid-base case closely follows the geostatic lateral earth pressure distribution, enabling a direct comparison between stress

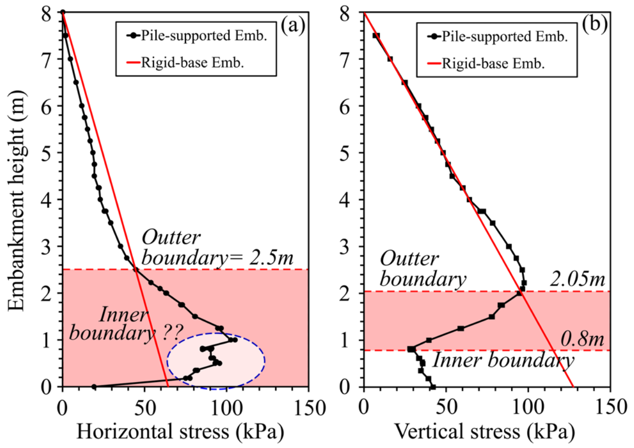

Fig. 3 Comparison between arching height determination methods: (a) Horizontal stress, and (b) vertical stress

redistribution with and without subsoil deformation. Using the conventional lateral stress method, the upper arch boundary is located 2.5 m above the embankment base. However, the lower boundary is ambiguous due to multiple stress fluctuations between 1.0 m and 0.5 m, including local stress increases. In full-scale embankment models with distant boundaries and significant lateral deformation, this oversimplified stress-based approach fails to provide a reliable, consistent definition of arch geometry, underscoring the need for a revised interpretation method.

Arch height is also commonly evaluated using vertical stress profiles for the same 8 m high embankment with 4*a* pile spacing (Fig. 3(b)). In this case, the piled and rigid-base models show good agreement in the upper half of the fill, indicating an approximately at-rest stress state and the absence of arching. A slight increase in vertical stress occurs between 4.0 m and 2.2 m above the piles, followed by a sharp reduction from 2.2 m to 0.8 m, marking the active arching zone and its lower boundary. Below this level, vertical stress increases parallel to the geostatic profile. Comparison with the lateral stress method reveals contradictory arch geometries, suggesting that a vertical stress–based approach provides more realistic estimates of arch height; however, it cannot predict the lower or inner boundary of the arch.

The lateral earth pressure coefficient (K) has also been used to interpret arching behavior, but existing studies restrict its application to vertical cross-sections within a central unit cell. As a dimensionless ratio incorporating both vertical and horizontal stresses, K enables clear contour visualization, with sharp gradients often associated with principal stress rotation and shearing.

Fig. 4(a) shows the variation of the lateral earth pressure coefficient, , along the embankment centerline for the 8 m high model with 4*a* pile spacing. From the embankment crown to 2.4 m above the piles, K remains below K_0 and approaches K_a, indicating lateral stress relaxation.

Earlier studies reported that the K-value follows the K_0 line from the arch crown to the embankment crest, then deviates upon entering the compression (arching) zone [3, 21, 22, 27]. In contrast, the present results show that from the crest down to the apex of the compression zone, the K-value does not match the K_0 line but instead aligns closely with the K_a line (Fig. 4(a)). As demonstrated in the methodology, the vertical stress distribution in this region corresponds to the geostatic vertical stress line, whereas the horizontal stress distribution falls below the geostatic curve, indicating unloading or relaxation. Comparing the two models suggests that this inconsistency arises from differences in boundary conditions and modeling approaches. To test this, instead of analyzing an entire embankment, the embankment was re-simulated using only the central unit cell (two central piles with the subsoil) and rigid side boundaries fixed against horizontal movement, consistent with common numerical approaches in the literature (Fig. 5(a)).

The results of the K value variations along the centerline cross-section of the above-mentioned model are presented in Fig. 5(b). The results show that, due to the model's rigid side boundaries, no horizontal displacement occurs in the fill, so the soil settles only in the vertical direction. Due to these constraints, both horizontal and vertical stresses will

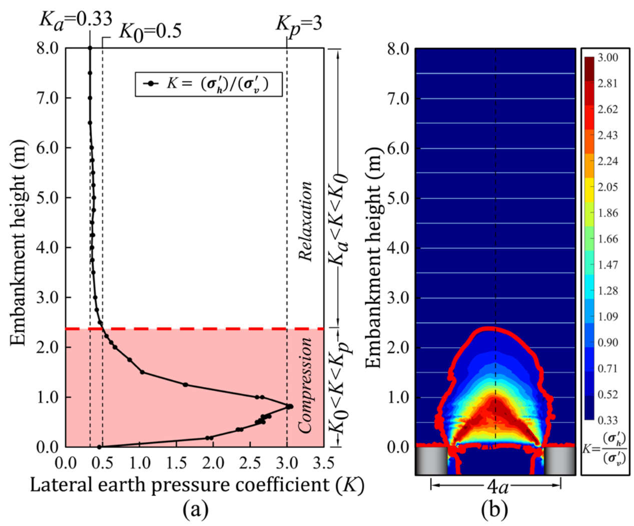

Fig. 4 Comparison between available and developed K-based arching shape determination methods for the 8 m high embankment with a pile spacing of 4*a*: (a) Defined compression and relaxation zones based on K variation, and (b) Lateral earth pressure coefficient contours and K_0 iso-line

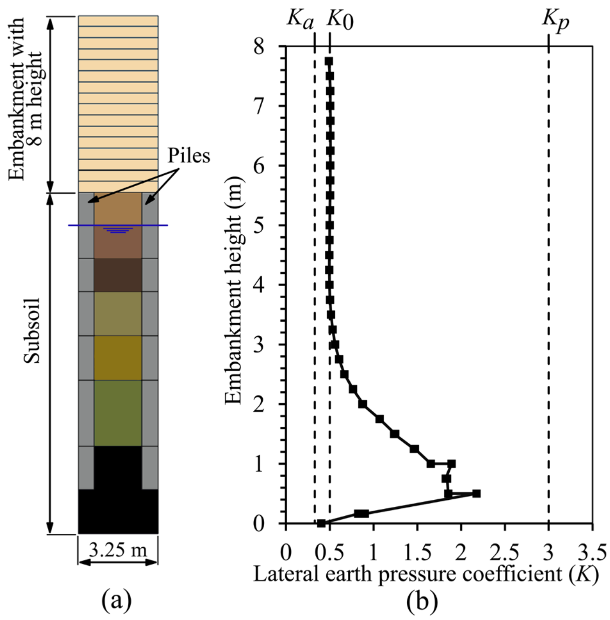

Fig. 5 Unit cell model for an 8 m-high embankment with 4*a* pile spacing: (a) The unit cell model and the subsoil, and (b) *K* value variation along the model's vertical centerline

follow their geostatic counterparts above the compression (arching) zone. As shown in Fig. 5(b), the *K* curves match the K_0 line from 3.75 m (the arch height) to 8 m, showing the same trend as reported in the literature [3, 21, 22, 25–27]. Another difference between the *K* curves of the full-scale model and the fixed-boundary model is the maximum *K* value. Also, the arch height in the model with fixed sides is 3.75 m; however, the same parameter is only 2.4 m in the full-scale model. Considering the significant difference between the arch height values of the tested models (1.35 m difference), it could be concluded that using the method that limits the horizontal displacements in the embankment body and only permits the vertical settlements could yield contradictory results, which could not be used to understand and explain the behavior of the whole embankment. If 3.75 m is assumed as the arch height, which consequently defines the location of the equal-settlement plane, the minimum embankment height required for mobilization of full arching and for limiting differential settlements at the embankment crest to negligible values become significantly larger. These required heights are much greater than those obtained from the more realistic model, assuming an arch height of 2.4 m.

A new approach is proposed in this paper for determining the arch geometry by combining *K* contours and K_0 isolines. According to this method to generate the *K* contours (Fig. 4(b)), the values of horizontal and vertical stresses along the embankment body were derived from the FEM analyses, and the K value was calculated using the following formula: $K = \sigma'_h / \sigma'_v$

Using an exclusive MATLAB [28] code, the calculated *K* values were used to generate the *K* contours. As illustrated in Fig. 4(b), among the numerous *K* contours, the isoline corresponding to the K_0 state is shown in red. The K_0 value was calculated based on the internal friction angle of the embankment fill material using the well-known equation of ($K_0 = 1 - \sin\phi'$).

4 Comparison and evaluation of analytical methods for the design of pile-supported embankments

A parametric investigation was conducted to enable a systematic comparison of the available design methods and to evaluate them against numerical finite element analyses. The study considers six design approaches for piled embankments, with the analysis extended to include different pile spacings (4*a*, 5*a*, and 6*a*) and embankment heights ranging from 2 m to 12 m. To ensure a consistent comparison, other parameters, including the soil unit weight, internal friction angle, and pile diameter, were held constant throughout the parametric evaluation of the design approaches.

The aim was to assess how predictions from different design methods respond to changes in individual parameters by comparing them with numerical analysis results. In each analysis, one parameter was varied at a time, while all other parameters were kept at their baseline values.

Since the referenced design methods are intended for practical three-dimensional applications, the outcomes obtained from two-dimensional FEM analyses were evaluated by comparison with the corresponding three-dimensional stress reduction ratio (S_{3D}). Introduced by Low et al. [29], the stress reduction ratio (SRR or S_{3D}) is defined as the ratio of the average vertical pressure acting on the subsoil at the clear span between two adjacent piles to the total weight of the soil column above that level [14]. Lower SRR values indicate greater arching. At the clear spacing between the central piles, a horizontal cross-section was taken at the bottom of the fill to record the stress values throughout the construction process, from the beginning of fill construction to the end of the final consolidation phase. The mean vertical stress obtained from this cross-section represents the pressure acting on the subsoil, and, with the embankment height considered, the SRR was calculated using the following equation:

$$\text{SRR} = S_{3D} = \sigma_v / \gamma H , \quad (1)$$

where σ_v is the average vertical stress over the sub-soil, γ is the unit weight of the soil, and H is the embankment height.

4.1 Design and analytical methods for the piled embankments

4.1.1 Terzaghi Method

The Terzaghi [2] model is classified as a friction-based soil arching model. This approach is developed based on the well-known trapdoor test. The equilibrium equations were derived using the weight of the moving rectangular soil block, the loads acting on it, and the shear resistance, all according to the Mohr-Coulomb failure criterion. Russell and Pierpoint [30] extended the Terzaghi model to include a third dimension, where the S_{3D} will be calculated as:

$$S_{3D} = \frac{s^2 - a^2}{4HaK\tan\phi'}\left(1 - e^{\frac{-4HaK\tan\phi'}{s^2 - a^2}}\right), \quad (2)$$

where s is the pile spacing, a is the pile width, H is the embankment height, and ϕ' is the internal friction angle of the soil.

4.1.2 Hewlett and Randolph Method

In contemporary piled embankment design practice, one of the most established approaches (limit-state equilibrium) is the method proposed by Hewlett and Randolph [10]. This analytical framework was later incorporated into BS8006-1 [31] as an alternative to the earlier empirical procedure originally presented in that standard.

Hewlett and Randolph [10] describe the soil arching mechanism within a pile grid as a succession of hemispherical dome-shaped zones or semispherical arches, each having a radius equal to half of the diagonal pile spacing. Failure of these arching zones is assumed to initiate at the dome apex or at the pile cap level, depending on the governing condition. Expressions for arching efficiency were subsequently formulated, and, based on these two limit conditions, the corresponding relationships for the stress-reduction ratio are presented below.

For the arch crown condition:

$$S_{3D} = \left(1 - \frac{a}{s}\right)^{2(K_p - 1)}\left(1 - \frac{s \times 2(K_p - 1)}{\sqrt{2}H(2K_p - 3)}\right) + \frac{(s-a)2(K_p - 1)}{\sqrt{2}H(2K_p - 3)} \quad (3)$$

For the pile cap condition:

$$S_{3D} = \frac{1}{\left(\frac{2K_p}{K_p + 1}\right)\left[\left(1 - \frac{a}{s}\right)^{(1-K_p)} - \left(1 - \frac{a}{s}\right)\left(1 + \frac{a}{s}K_p\right)\right] + \left(1 - \frac{a^2}{s^2}\right)}$$

$$K_p = (1 + \sin\varphi')/(1 - \sin\varphi')$$

γ is the soil unit weight, s is the center-to-center pile spacing, a is the pile width, K_p is the passive lateral earth pressure coefficient, and H is the height of the embankment fill.

4.1.3 Low et al. Method

Low et al. [29] examined a piled embankment configuration incorporating pile caps together with the contribution of the subsoil. Their work extended the approach of Hewlett and Randolph [10] by introducing a body force term into the plane-strain differential equation of equilibrium, thereby refining the analytical representation of the system. The thickness of each arch is equal to half the pile width. Stress reduction ratio can be calculated as:

$$S_{3D} = \frac{\frac{\gamma(s-a)(K_p - 1)}{2(K_p - 2)} + \left(\frac{s-a}{s}\right)^{K_p - 1}\left[\gamma H - \frac{\gamma s}{2}\left(1 + \frac{1}{K_p - 2}\right)\right]}{\gamma H}, \quad (4)$$

where γ is the soil unit weight, s is the center-to-center pile spacing, a is the pile width, K_p is the passive lateral earth pressure coefficient, and H is the height of the embankment fill.

4.1.4 Kempfert et al. Method

Another widely applied limit-state equilibrium-based approach is detailed by Kempfert et al. [11]. This approach was subsequently incorporated into the EBGEO [32]. This approach was established through three-dimensional physical model investigations that accounted for the influence of reinforcement and the supporting subsoil. The arching mechanism is represented as a sequence of non-concentric arches, or multiple shells, with the outermost and largest arch assumed to reach a height equivalent to one-half of the radial spacing between piles. The corresponding expression for the stress-reduction ratio using this method is presented below.

$$S_{3D} = \frac{1}{\gamma H}\left\{\lambda_1^x\left(\gamma+\frac{q}{H}\right)\left[\begin{array}{l} H\left(\lambda_1+h_g^2\lambda_2\right)^{-x} \\ +h_g\left(\frac{\lambda_1+h_g^2\lambda_2}{4}\right)^{-x} \\ -h_g\left(\lambda_1+h_g^2\lambda_2\right)^{-x} \end{array}\right]\right\}, \quad (5)$$

where:

$$\lambda_1 = \frac{1}{8}\left(s_d-a\right)^2,$$

$$\lambda_2 = \frac{s_d^2+2ds_d-a^2}{2s_d^2},$$

$$x = \frac{d\left(K_p-1\right)}{\lambda_2 s_d},$$

$$h_g = s_d/2 \quad \text{for} \quad H \geq s_d/2,$$

$$h_g = H \quad \text{for} \quad H < s_d/2$$

In this formulation, h_g is the arching height, q refers to the applied surcharge (considered as zero in the current study, only the self-weight of the fill), H indicates the embankment height, γ is the unit weight of the embankment material, and s_d corresponds to the diagonal center-to-center spacing between piles.

4.1.5 BS 8006-1 and BS 8006-modified Method

BS8006-1 [31] and BS8006-modified [33] determine the mean vertical stress imposed on the piles using the formulation for positive projecting conduits. Furthermore, BS8006-1 [31] provides empirical relationships for estimating the arching coefficient, C_c, as outlined below.

This model is of significant importance due to its extensive use in practical design. In determining the vertical stress at the base of the embankment, BS8006-1 [31] distinguishes between two conditions. The first applies when the embankment height is greater than 0.7(s−a) and less than the critical value of 1.4(s−a), under which partial soil arching is assumed to occur within the fill. The second condition corresponds to embankment heights equal to or exceeding 1.4(s−a), assuming full arching (as used in the current parametric study) is established. Beyond this threshold, any additional vertical load resulting from further increases in embankment height is assumed to be transferred directly to the piles. Expressions for the stress-reduction ratio for both conditions can be formulated using the procedure presented by Russell and Pierpoint [30].

For full arching:

$$S_{3D} = \frac{2.8s}{\left(s+a\right)^2 H}\left[s^2-a^2\left(\frac{P_C}{\gamma H}\right)\right], \quad \left(\frac{P_C}{\gamma H}\right) = \left(\frac{C_c a}{H}\right)^2, \quad (6)$$

where C_c is the arching coefficient, and P_c is the vertical stress acting on the pile. For the end-bearing piles used in this embankment: C_c = 1.95 (H / a) − 0.18

5 Results and discussion

5.1 *K* contours for high embankments

Fig. 6 shows the color contours of the lateral earth pressure coefficient (K) at the central section of the unreinforced piled embankments with the height of 6 m, 8 m, and 10 m and the pile spacings of 4a, 5a, and 6a. Additionally, an isoline representing K = K_0 is drawn in red over the contours. The K = K_0 isoline clearly delineated the arching

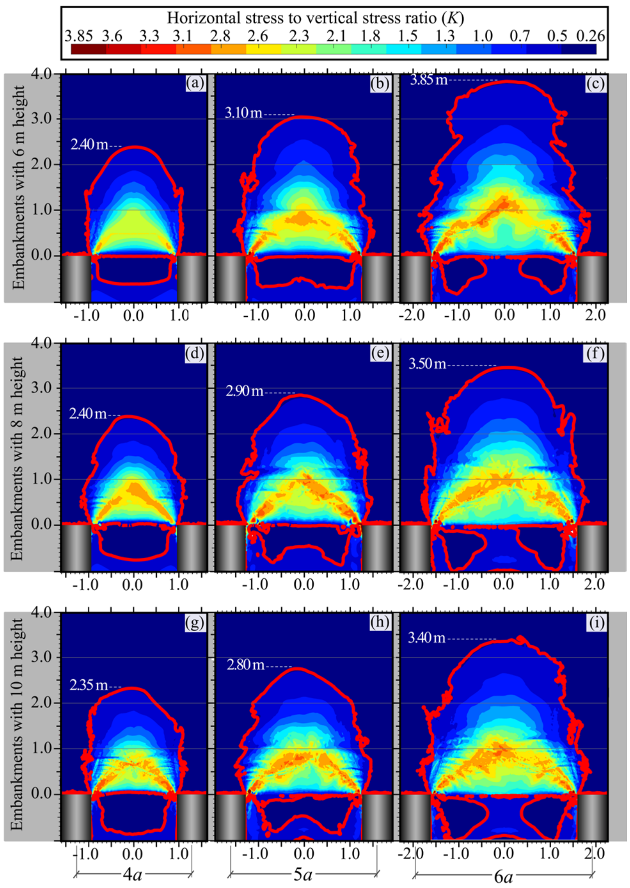

Fig. 6 The K contours and the shape of the formed arch at the center of the CPS embankments characterized by the K_0 isoline for: (a) 6H-4a, (b) 6H-5a, (c) 6H-6a, (d) 8H-4a, (e) 8H-5a, (f) 8H-6a, (g) 10H-4a, (h) 10H-5a, (i) 10H-6a

region, separating the compressed arching zone from the surrounding relaxation zone ($K < K_0$), providing a reliable method for identifying arch geometry. Unlike previous studies that inferred arch height indirectly [3, 21, 21, 25–27], this approach directly defines the compression zone. For a constant fill height, increasing pile spacing increases arch height, whereas increasing fill height generally reduces it. Near the pile heads, $K < K_0$ dominates due to higher vertical stresses, producing behavior analogous to an active wedge beneath a foundation. In regions where $K < K_0$, soil behavior is governed by lateral expansion above the arches and vertical compression, particularly near pile heads. The arching zone comprises multiple arches with varying degrees of compression, resembling the multi-shell arching concept of the German model [4]. For the 4*a* pile spacing, the arch height is largely insensitive to embankment height. As expected, wider pile spacing increases arch height, with this effect being more pronounced at lower embankment heights.

5.2 *K* contours for low-height CPS Embankments

Fig. 7 shows the color contours of the lateral earth pressure coefficient (K) at the central section of the CPS embankments with a height of 2 m and 4 m, as well as a pile spacing of 4*a*, 5*a*, and 6*a*.

For 2 m high reinforced and non-reinforced embankments, insufficient fill height prevents arch formation for all pile spacings, causing shear bands to extend vertically from pile edges to the surface and directly transmit subsoil settlement to the crest, consistent with shear-plane

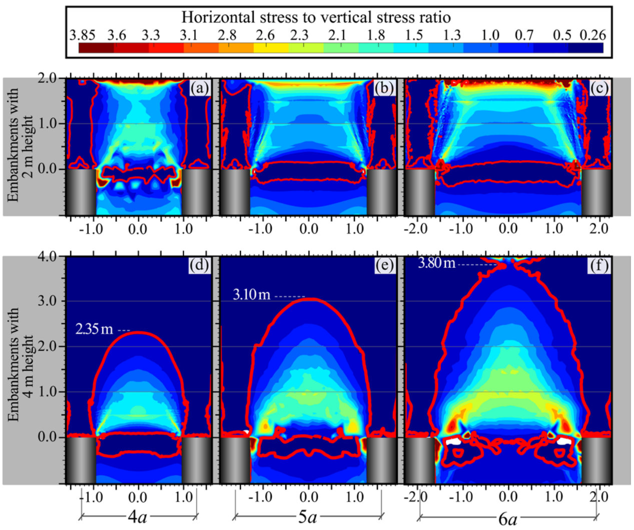

Fig. 7 The K contours and the shape of the formed arch at the center of the modeled low embankments characterized by the K_0 isoline for: (a) 2*H*-4*a*, (b) 2*H*-5*a*, (c) 2*H*-6*a*, (d) 4*H*-4*a*, (e) 4*H*-5*a*, and (f) 4*H*-6*a*

arching. In 4 m-high non-reinforced embankments, full arching develops for 4*a* and 5*a* spacing, whereas only partial arching occurs at 6*a* spacing [18, 21, 22, 27].

5.3 Stress reduction ratio (SRR) - Trapdoor physical models and piled embankments

The progressive development of the soil arching ratio with respect to the trapdoor's relative displacement has been identified in both theoretical and experimental studies [14, 18, 21, 22, 27]. This evolution can be represented by a ground reaction curve (GRC). The GRC can represent the changes of the SRR versus trapdoor displacement normalized by the trapdoor width, which typically consists of four distinct stages: (*i*) initial soil arching, (*ii*) maximum soil arching, corresponding to the minimum SRR, (*iii*) stress recovery, and (*iv*) the ultimate state, corresponding to the ultimate SRR. However, the Ground Reaction Curve (GRC) concept cannot be directly applied to real embankments.

In a trapdoor test, the trapdoor remains fixed throughout the construction of the fill and is only lowered gradually after the fill has been fully placed, allowing measurement of the acting stresses and corresponding settlements. In recent three-dimensional physical model studies, peat layers or water-saturated foam rubber cushions have been employed to simulate gradual subsoil settlement. However, unlike actual field conditions, consolidation processes during embankment construction and surcharge application were not considered. In contrast, in a real embankment, settlement of the underlying subsoil occurs from the earliest stages of fill placement. Due to this fundamental difference, the shape and evolution of GRCs derived from trapdoor experiments differ significantly from those observed in real embankments. Moreover, while the trapdoor test begins from a fully loaded condition, embankment construction occurs in stages, with the load on the subsoil increasing progressively as each fill layer is placed.

Fig. 8 [8, 10, 29, 31–33] illustrates the comparative variation in the stress-reduction ratio (SRR) with embankment height normalized by the clear pile spacing for FEM models and the studied piled embankment design methods, considering each pile spacing. To the authors' knowledge, this study is the first to present the progressive development of soil arching and the associated redistribution of stresses between the piles and the sub-soil at each stage of embankment construction.

Stress reduction ratios are evaluated independently for each design approach by varying the pile spacing and embankment height. The results from the different

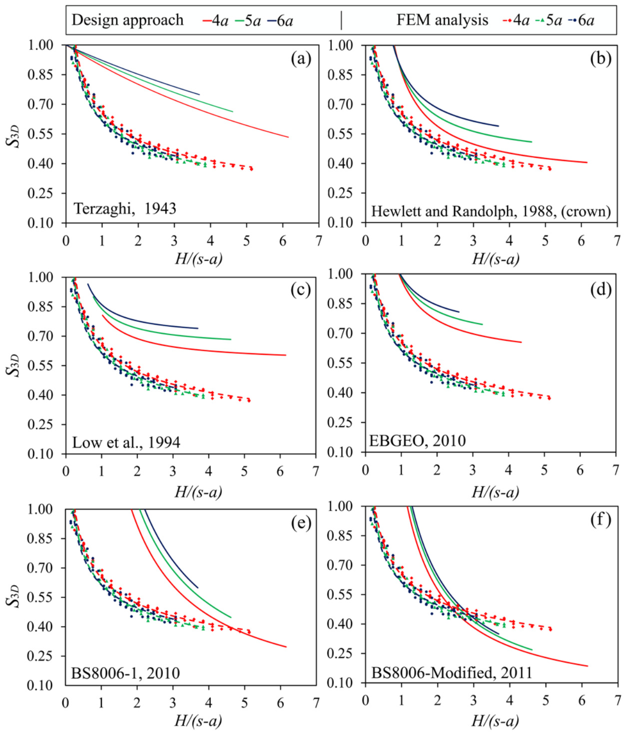

Fig. 8 Comparative numerical and analytical SRR values variation at the central sub-soil span versus normalized embankment height with respect to the clear pile spacing (a) Terzaghi [8], (b) Hewlett and Randolph [10] (arch crown), (c) Low et al. [29], (d) EBGEO [32], (e) BS8006-1 [31], and (f) BS8006-Modified [33]

design methods are then assessed by comparing them with stress-reduction ratios derived from two-dimensional FEM simulations. In the graphical representation of the S_{3D} for analytical approaches, values greater than 1 are masked, as S_{3D} = 1 indicates no arching. So, the arching behavior differs significantly among the design approaches for low embankments. This happens because of the different assumptions and logics of each design method.

It is noteworthy that among the limit-state equilibrium framework approaches, three of them (Hewlett and Randolph, BS8006-1, BS8006-Modified) provide a more effective basis for evaluating soil arching in embankments.

Across all analytical approaches, except BS8006-Modified, models with smaller pile spacing have lower S_{3D} values, indicating more efficient arching. However, FEM results show very similar behavior of the S_{3D} trend across all pile spacings as the fill height increases. It should be noted that across all pile spacings, the FEM models initially exhibit a sharp decrease in SRR, indicating a progressive increase in arching and a greater load transfer to the piles. Beyond a certain point, the SRR value decreases gradually as additional fill layers are added.

The Hewlett and Randolph approach yields the closest behavior and S_{3D} trend among all design approaches compared to the FEM results. The Terzaghi [2] and EBGEO [32] methods significantly underpredict S_{3D}, making these approaches highly conservative.

Fig. 9 [8, 10, 29, 31–33] illustrates the variation of S_{3D} with center-to-center pile spacing normalized by the clear pile spacing for FEM models and piled embankment design approaches, considering each fill height. As expected in all models, increasing fill height decreases S_{3D} values; however, the sensitivity of S_{3D} to height changes differs significantly between models. The BS8006-1 and BS8006-Modified methods are highly sensitive to changes in embankment height, as there is a considerable difference in the SRR between 10 m and 2 m-high fills across all pile spacings. For some models, such as BS8006-1, BS8006-Modified, and EBGEO, the S_{3D} curves for fill heights of 2 and 3 m are not shown because they fall outside the valid range (0-1). BS8006-1, BS8006-Modified, and the Hewlett and Randolph models showed the best agreement with the FEM analysis results. Also, it can be seen that after a specific value, the increase in fill height due to construction does not significantly affect the S_{3D} value. This behavior

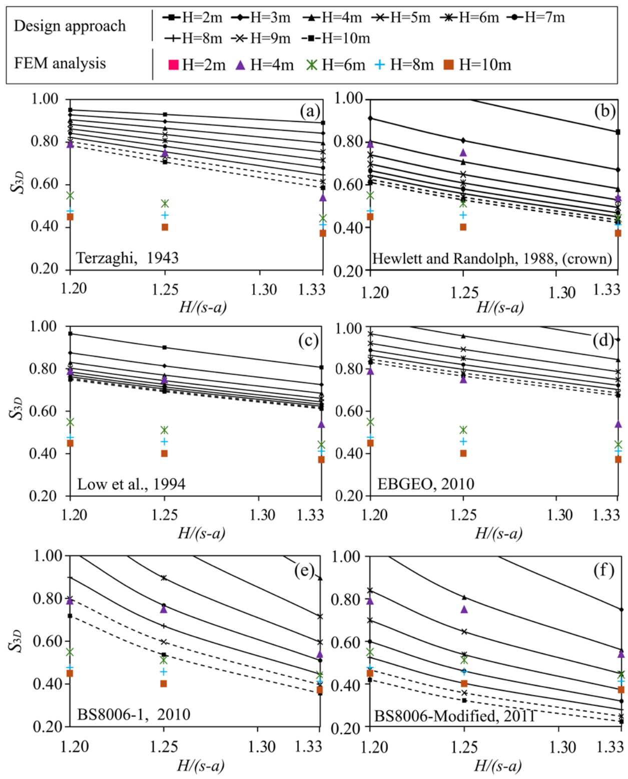

Fig. 9 Variation of S_{3D} with center-to-center pile spacing normalized by the clear pile spacing for FEM models and piled embankment design approaches, considering fill height: respect to the clear pile spacing (a) Terzaghi [8], (b) Hewlett and Randolph [10] (arch crown), (c) Low et al. [29], (d) EBGEO[32], (e) BS8006-1 [31], and (f) BS8006-Modified [33]

is also confirmed by the FEM results, where, after initial construction stages, the decrease in S_{3D} with increasing fill height occurs at a much lower rate. It could be due to the formation of the full arch, which does not change with further fill construction.

5.4 Arch evolution during embankment construction

Fig. 10 shows the progressive, stepwise formation and evolution of the arches within the embankment fill for the model with an 8 m height and 5*a* pile spacing. The visible height for the study area is shown as a range from the central pile heads to 4 m above them. There are 3 sets of isolines for lateral earth pressure coefficients (K).

The isolines represented by shades of black correspond to the relaxation zone with $0.33 < K < 0.5$. The compression zone ($0.5 < K < 3$) or the region where arching is formed above the subsoil due to lateral extrusion and the plugging effect of the particles is shown in shades of red. The thick red isoline represents $K_0 = 0.5$, which is the boundary of the arch separating the relaxation and compression zones. Using this novel method, not only could the precise shape and geometry of the arch be determined, but it also sheds light on the mechanical explanation of the redistribution in the piled embankments. Also, the shape of the isolines within the arching region is well aligned with the assumptions of the multi-shell non-concentric model by Kempfert et al. [11], which served as the basis for German EBGEO.

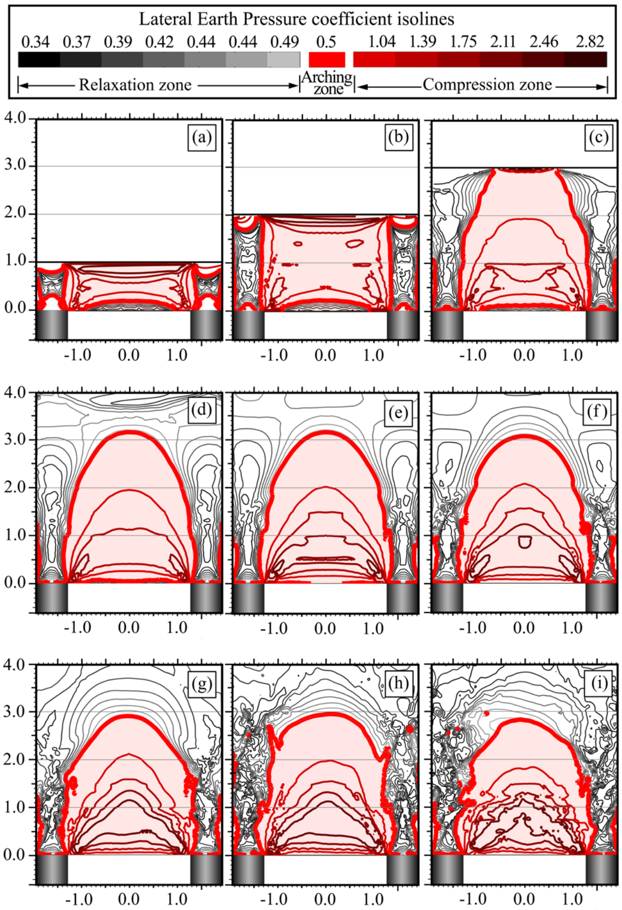

Fig. 10 Arching evolution for the model with an 8 m height and 5*a* pile spacing for the fill construction heights of: (a) 1 m, (b) 2 m, (c) 3 m, (d) 4 m, (e) 5 m, (f) 6 m, (g) 7 m, (h) 8 m, and (i) the end of consolidation

Starting from a height of 1 m, each stage shows 1 m of embankment construction, up to the final 8 m height. The Figs. 10(a) and 10(b) show that due to the insufficient height of the fill, the arching type is shear-plane arching, where the deformations in the subsoil will be directly reflected on the fill surface. However, as the fill height increases gradually, the arch starts to form and becomes a partial arch in Fig. 10(c), where the arch force bridges tend to overlap above the settling subsoil. Starting from a 4 m embankment height, the arch evolves from partial to full arching, and its height increases to a maximum of 3.25 m (Figs. 10(d) and 10(e)). By continuing the fill construction, the overburden pressure on the arch structure increases, and as the arch remains a full arch, its height decreases to a final height of 2.8 m for the fill height of 8 m (Figs. 10(f), 10(g), and 10(h)). In a full arching case, the subsoil settlement will have a negligible effect on surface differential settlement in the fill. Also, a final full consolidation phase has a negligible effect on the formed arch (Fig. 10(i)).

5.5 Critical embankment height - Comparison of the proposed methodology with existing approaches

An important parameter in the design of piled embankments is the critical embankment height, defined as the minimum fill height required for full arch formation [18]. Various methods proposed in the literature for estimating this height are summarized in Fig. 11 [7–11, 18, 19, 29, 31, 32, 34–46], all of which relate the critical height to the clear pile spacing (s–a), where s is the center-to-center pile spacing, and a is the pile width. Also, Fig. 11 [7–11, 18, 19, 29, 31, 32, 34–46] compares the critical heights obtained in the current study with those predicted by existing analytical methods for 4*a*, 5*a*, and 6*a* pile spacing. Although substantial discrepancies exist among the analytical predictions, the critical height ranges derived from the present numerical models fall near the center of the overall distribution, as indicated by the red dashed zones.

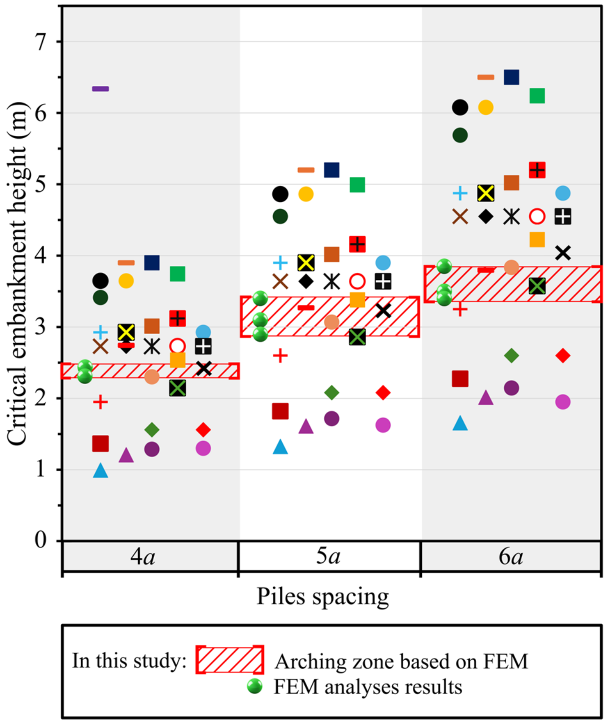

Method	Critical Height	4*a*	5*a*	6*a*
Terzaghi [8]	2.0 (*s-a*)	3.90	5.20	6.50
Carlson [34]	1.87 (*s-a*)	3.64	4.86	6.07
Hewlett and Randolph [10]	1.4 (*s-a*)	2.73	3.64	4.55
Low et al. [29]	1.4 (*s-a*)	2.73	3.64	4.55
BS 8006 [35]	1.4 (*s-a*)	2.73	3.64	4.55
Horgan and Sarby [36] - Lower	1.92 (*s-a*)	3.01	4.01	5.02
Horgan and Sarby [36] - Upper	1.545 (*s-a*)	3.74	4.99	6.24
Han and Gabr [37]	1.3 (*s-a*)	2.53	3.38	4.22
Nordic NGG [38]	1.87 (*s-a*)	3.64	4.86	6.07
Kempfert et al. [11]	*s*/2	1.30	1.62	1.95
Jenck et al. [39]	1.5 (*s-a*)	2.92	3.90	4.87
Chen et al. [9] - Lower	1.6 (*s-a*)	2.73	3.64	4.55
Chen et al. [9] - Upper	1.4 (*s-a*)	3.12	4.16	5.20
Naughton [40]	C (*s-a*)*	2.41	3.22	4.02
Chen et al. [41] - Lower	1.5(*s-a*)	1.95	2.60	3.25
Chen et al. [41] - Upper	1.0(*s-a*)	2.92	3.90	4.87
BS 8006-1 [31]	0.7 (*s-a*)	1.36	1.82	2.27
EBGEO [32]	0.8 (*s-a*)	1.56	2.08	2.60
Van Eekelen et al. [7] - Lower	0.62 (*s-a*)	0.99	1.32	1.65
Van Eekelen et al. [7] - Upper	0.51 (*s-a*)	1.20	1.61	2.01
Xu et al. [42] - Lower	1.5(*s-a*)	2.14	2.86	3.57
Xu et al. [42] - Upper	1.1 (*s-a*)	2.92	3.90	4.87
CUR 226 [43]	0.66 (*s-a*)	1.28	1.72	2.14
Rui et al. [19]	1.75 (*s-a*)	3.41	4.55	5.68
Lai et al. [18]	0.8 (*s-a*)	1.56	2.08	2.60
Filz et al. [44]	0.81 *s* + 0.98 *a*	2.74	3.26	3.79
Lee et al. [45] - Lower	3.25 (*s-a*)	3.90	5.20	6.50
Lee et al. [45] - Upper	2.0 (*s-a*)	6.33	8.45	10.5
Samira et al. [46]	1.18 (*s-a*)	2.30	3.06	3.83

*$C=0.5e^{(\pi/2)\tan\phi}$

Fig. 11 Critical embankment height variation considering the available correlations in the literature compared to the results of the current study

5.6 Equal-settlement plane derived from the behavior of full-scale embankments

The equal settlement plane (ESP) is the plane above which there would be almost no differential settlement caused by the subsoil settlement in the piled embankments. The height of the equal settlement plane for the piled embankment models could be evaluated by analyzing the vertical displacements along the height of the embankment at two critical locations, directly above the center of the pile and at the mid-span between adjacent piles (at the central section of the embankment). As expected, in the unit-cell models available in the literature, larger settlements occur at the mid-span between adjacent piles, whereas the settlements at the pile heads are nearly zero at the pile head level for embedded piles. Moving farther from the pile's level due to arching and the reorientation of principal stresses, the settlement and deformation patterns will, however, differ. Consequently, settlements along the mid-pile axis tend to increase, while those along the axis passing through the mid-span between piles decrease. The level at which the settlements along these two axes equalize is defined as the equal settlement plane. This approach is commonly adopted in literature to determine the height of the equal-settlement plane in centrifuge and finite element (FE) models with rigid boundary conditions [6, 47, 48] and full-sized embankment FE models [12].

This method has been validated primarily for unit-cell models with rigid boundaries, which neglect lateral spreading effects. This limitation, central to the present study, was also highlighted by Smith et al. [47].

In the current study, the use of a full-scale model with distant side boundaries enabled the realistic modeling of lateral deformations, resulting in a distinct vertical displacement pattern, as shown in Fig. 12, compared to patterns reported in the literature [6, 47, 48].

Fig. 12(a) presents settlement profiles for full-scale CPS embankments with a height of 6 m and pile spacings of 4*a*, 5*a*, and 6*a*. The rightward-leaning curves indicate continued settlement above the curve intersection, with settlement rates varying by pile spacing despite identical embankment heights. This behavior agrees with full-scale physical modeling results reported by Bian et al. [12]. For 4*a* spacing, the equal-settlement plane occurs at approximately 2.65 m, 2.60 m, and 2.40 m for embankment heights of 6 m, 8 m, and 10 m, respectively.

For embankments with larger pile spacings (5*a* and 6*a*), settlement curves continue to diverge above their first intersection, indicating the absence of a true equal settlement plane. Instead, "differential settlement prediction planes" can be defined at any elevation to quantify differential settlement. This demonstrates that the equal settlement plane is distinct from arch height and critical embankment

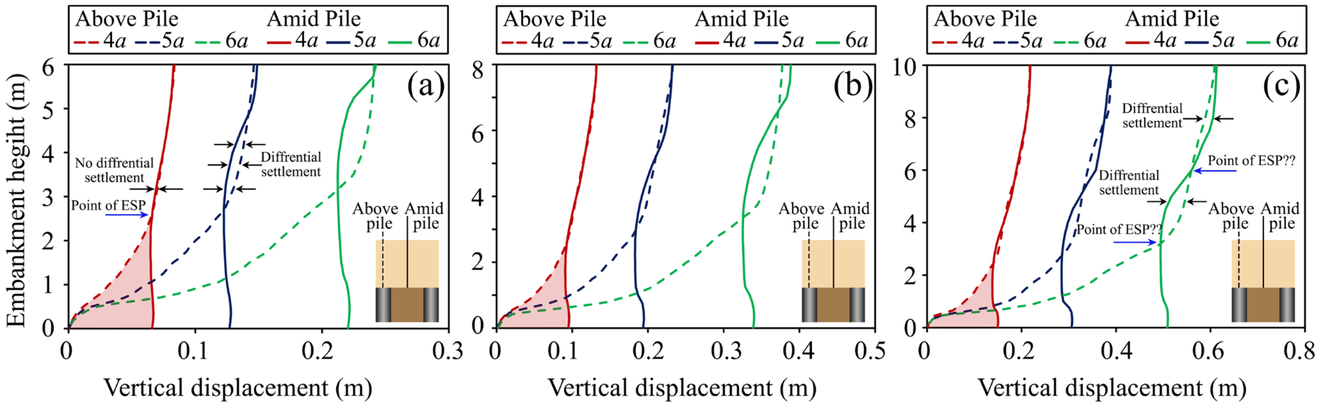

Fig. 12 Vertical displacements within models along the cross-sections above pile and amid piles: (a) 6 m; (b) 8 m; and (c) 10 m high embankments

height, and that differential settlements may persist even at critical height, particularly in more flexible systems with wider pile spacing (Figs. 12(a), 12(b), and 12(c)).

6 Conclusions

The arching mechanism, which can be described as the transfer of stresses from a yielding soil zone to adjacent less yielding zones, is a crucial aspect to be considered in the analysis and design of piled embankments constructed on soft soils. There is considerable research aimed at understanding the arching mechanism; however, most studies rely on the unit-cell approach, which fails to account for lateral stresses and deformations. On the other hand, lateral spreading action is a prominent feature of embankments. This paper is based on parametric full-scale FE analyses to gain a clear understanding of the varying stress redistribution and arching mechanisms along the embankment. CPS embankments, both high and low, with different pile spacings, were analyzed. Arching evolution is illustrated using K-value contours with the K_0 isoline superimposed to define the full arch geometry. The K_0 isoline clearly separates compression and extension zones, providing a precise representation of arch shape and height. The full-scale embankment modeling approach, combined with the interpretation of arching evolution through K-value variation, has proven successful in revealing the complete formation of arches, including their maximum height. This, in turn, enables determination of the critical embankment height and its relationship to clear pile spacing, which are essential parameters for achieving a satisfactory, optimal design from a practical engineering perspective.

In addition to these, the following conclusions drawn from this study are also noteworthy for interpreting the behavior of piled embankments.

The analysis demonstrates the different stages of arching evolution. For low embankment heights ($H \leq 2$ m), shear-plane arching dominates, with subsoil deformations transmitted directly to the fill surface.

With increasing fill height, a transition from shear-plane arching → partial arching → full arching was observed.

At approximately $H = 4$ m, a full arch mechanism is established, marking a fundamental mechanical transition in load transfer behavior. The arch height increases progressively during formation, reaching a maximum value. After full arch establishment, additional fill height does not increase arch height; instead, overburden pressure causes a moderate reduction to a stabilized height

A comprehensive parametric evaluation was undertaken to systematically examine the performance of six established design approaches for piled embankments over a practical range of pile spacings and embankment heights. The methods were benchmarked against numerical finite element analyses using the three-dimensional stress reduction ratio (S_{3D}), providing a consistent, application-oriented assessment framework.

The study demonstrates that soil arching in piled embankments develops progressively during staged construction, rather than following the classical Ground Reaction Curve (GRC) derived from trapdoor experiments, which the tests begin from a fully loaded condition. Real embankments experience simultaneous loading and subsoil settlement from the earliest construction stages, leading to a distinct evolution of SRR.

Across all pile spacings, FEM predicts a pronounced early reduction in SRR (rapid arching development), followed by a gradual change with increasing height, indicating diminishing sensitivity once the arch stabilizes (full arching establishment). Among the analytical methods, Hewlett & Randolph best reproduces the FEM S_{3D} trend, while Terzaghi and EBGEO markedly underpredict S_{3D}

(conservative). Within the limit-state equilibrium family, Hewlett & Randolph, BS8006-1, and BS8006-Modified provide the most credible basis for arching assessment.

In arching studies, a generally accepted method exists for determining the equal settlement plane. The applicability of this method was tested in this paper, and it was found to be limited to the presence of closely spaced piles. For largely spaced piles, however, differential settlements continue to occur at much higher levels above the critical embankment height. Based on this finding, the notion of the equal settlement plane is revised in meaning and is proposed to be defined as lines of "differential settlement prediction".

From a practical engineering perspective, the embankments need to be designed so that their total height exceeds the critical embankment height. Once this threshold is exceeded, full arching is mobilized, ensuring optimal load transfer to the piles and significantly mitigating differential settlement at the pavement surface. The methodology proposed in this paper, which utilizes the *K*-value and compression-extension zoning, offers a reliable and precise approach to determining arch geometry using numerical modeling and considering the pile spacing, embankment height, and the fill material properties.

A natural and promising extension of this work could be the investigation of geosynthetic-reinforced piled embankments, where the core principles validated here can be applied to those systems. Future research can build upon these findings to integrate the effects of geogrid layers. Incorporating geogrid reinforcement, which is expected to restrict lateral expansion and alter earth pressure coefficients (K_0, K_a, and K_p), will enable the current methodology to be used to optimize designs with larger pile spacings and reduced pile cap dimensions.

Acknowledgements
The authors would like to thank the Scientific and Research Council of Turkey (TUBITAK) for supporting this study with project number 122M040.

References

[1] Feld, J. "Early history and bibliography of soil mechanics", In: Proceedings of the 2nd International Conference on Soil Mechanics and Foundation Engineering, Rotterdam, Netherlands, 1948, 1, pp. 1–7.

[2] Terzaghi, K. "Stress distribution in dry and in saturated sand above a yielding trapdoor", Harvard University Engineering Experiment Station, Cambridge, United States, Publication 99, 1936, pp. 1–11.

[3] Meena, N. K., Nimbalkar, S., Fatahi, B., Yang, G. "Effects of soil arching on behavior of pile-supported railway embankment: 2D FEM approach", Computers and Geotechnics, 123, 103601, 2020. https://doi.org/10.1016/j.compgeo.2020.103601

[4] Van Eekelen, S. J., Bezuijen, A., Lodder, H. J., Van Tol, A. F. "Model experiments on piled embankments. Part I", Geotextiles and Geomembranes, 32, pp. 69–81, 2012. https://doi.org/10.1016/j.geotexmem.2011.11.002

[5] Van Eekelen, S. J., Bezuijen, A., Lodder, H. J., Van Tol, A. F. "Model experiments on piled embankments. Part II", Geotextiles and Geomembranes, 32, pp. 82–94, 2012. https://doi.org/10.1016/j.geotexmem.2011.11.003

[6] King, L., Bouazza, A., Dubsky, S., Rowe, R. K., Gniel, J., Bui, H. H. "Kinematics of soil arching in piled embankments", Géotechnique, 69(11), pp. 941–958, 2019. https://doi.org/10.1680/jgeot.18.P.104

[7] Van Eekelen, S. J. M., Bezuijen, A., Van Tol, A. F. "An analytical model for arching in piled embankments", Geotextiles and Geomembranes, 39, pp. 78–102, 2013. https://doi.org/10.1016/j.geotexmem.2013.07.005

[8] Terzaghi, K. "Theoretical soil mechanics", John Wiley & Sons, 1943. ISBN 9780470172766 https://doi.org/10.1002/9780470172766

[9] Chen, Y. M., Cao, W. P., Chen, R. P. "An experimental investigation of soil arching within basal reinforced and unreinforced piled embankments", Geotextiles and Geomembranes, 26(2), pp. 164–174, 2008. https://doi.org/10.1016/j.geotexmem.2007.05.004

[10] Hewlett, W. J., Randolph, M. F. "Analysis of piled embankments", International Journal of Rock Mechanics and Mining Sciences and Geomechanics Abstracts, 25(6), pp. 297–298, 1988. https://doi.org/10.1016/0148-9062(88)91283-1

[11] Kempfert, H., Göbel, C., Alexiew, D., Heitz, C. "German recommendations for reinforced embankments on pile-similar elements", In: Proceedings of EuroGeo3, Munich, Germany, 2004, pp. 279–284.

[12] Bian, X., Liu, S., Duan, X., Jiang, J., Chen, Y. "Dynamic soil arching effect in pile-supported embankment due to train passages at high speeds", Soil Dynamics and Earthquake Engineering, 181, 108690, 2024. https://doi.org/10.1016/j.soildyn.2024.108690

[13] Al-Naddaf, M., Han, J., Jawad, S., Abdulrasool, G., Xu, C. "Investigation of stability of soil arching under surface loading using trapdoor model tests", In: Proceedings of the 19th International Conference on Soil Mechanics and Geotechnical Engineering, Seoul, South Korea, 2017, pp. 889–892.

[14] Han, J., Wang, F., Al-Naddaf, M., Xu, C. "Progressive development of two-dimensional soil arching with displacement", International Journal of Geomechanics, 17(12), 04017112, 2017. https://doi.org/10.1061/(ASCE)GM.1943-5622.0001025

[15] Rui, R., Han, J., Van Eekelen, S. J. M., Wan, Y. "Experimental investigation of soil-arching development in unreinforced and geosynthetic-reinforced pile-supported embankments", Journal of Geotechnical and Geoenvironmental Engineering, 145(1), 04018103, 2019. https://doi.org/10.1061/(ASCE)GT.1943-5606.0002000

[16] Rui, R., Van Tol, F., Xia, Y. Y., Van Eekelen, S., Hu, G. "Evolution of soil arching: 2D analytical models", International Journal of Geomechanics, 18(6), 04018056, 2018. https://doi.org/10.1061/(ASCE)GM.1943-5622.0001169

[17] Benmebarek, S., Berrabah, F., Benmebarek, N. "Effect of geosynthetic reinforced embankment on locally weak zones by numerical approach", Computers and Geotechnics, 65, pp. 115–125, 2015. https://doi.org/10.1016/j.compgeo.2014.12.004

[18] Lai, H. J., Zheng, J. J., Zhang, R. J., Cui, M. J. "Classification and characteristics of soil arching structures in pile-supported embankments", Computers and Geotechnics, 98, pp. 153–171, 2018. https://doi.org/10.1016/j.compgeo.2018.02.007

[19] Rui, R., Van Tol, F., Xia, X. L., Van Eekelen, S., Hu, G., Xia, Y. Y. "Evolution of soil arching: 2D DEM simulations", Computers and Geotechnics, 73, pp. 199–209, 2016. https://doi.org/10.1016/j.compgeo.2015.12.006

[20] Bentley "PLAXIS 2D, (Version 2025)", [computer program] Available at: https://www.bentley.com/software/plaxis-2d/ [Accessed: 07 June 2026]

[21] Salimnezhad, A., Almasraf, M., Çinicioğlu, Ö., Çinicioğlu, F. "Comparative evaluation of arching mechanisms in low- and high-rise embankments", Turkish Journal of Civil Engineering, 37(3), pp. 81–104, 2026. https://doi.org/10.18400/tjce.1816915

[22] Almasraf, M., Salimnezhad, A., Kelek, B. E., Çinicioğlu, O., Çinicioğlu, S. F. "A comparative discussion on soil arching evolution in CPS and GRPS embankments", In: Geotechnical Engineering Challenges to Meet Current and Emerging Needs of Society, CRC Press, 2024, pp. 295–300. ISBN 9781003431749 https://doi.org/10.1201/9781003431749-28

[23] Oztoprak, S., Çinicioğlu, S. F. "Looking into an appropriate methodology for the embankment design and construction on soft soils", Lowland Technology International, 9(2), pp. 21–28, 2007.

[24] Hird, C. C., Pyrah, I. C., Russell, D., Çinicioğlu, F. J. C. "Modelling the effect of vertical drains in two-dimensional finite element analyses of embankments on soft ground", Canadian Geotechnical Journal, 32(5), pp. 795–807, 1995. https://doi.org/10.1139/t95-077

[25] Wijerathna, M., Liyanapathirana, D. S. "Load transfer mechanism in geosynthetic-reinforced column-supported embankments", Geosynthetics International, 27(3), pp. 236–248, 2020. https://doi.org/10.1680/jgein.19.00022

[26] Ye, G. B., Wang, M., Zhang, Z., Han, J., Xu, C. "Geosynthetic-reinforced pile-supported embankments with caps in a triangular pattern over soft clay", Geotextiles and Geomembranes, 48(1), pp. 52–61, 2020. https://doi.org/10.1016/j.geotexmem.2019.103504

[27] Salimnezhad, A., Almasraf, M., Çinicioğlu, S. F., Çinicioğlu, O. "Investigating the effects of lateral deformations in CPS embankments on soil arching: a parametric study using finite element analysis", presented at 9th Geotechnical Symposium, Istanbul, Turkey, Nov. 22–24, 2023. https://doi.org/10.5505/2023geoteknik.SS-22

[28] The MathWorks, Inc. "MATLAB, (R2021a)", [computer program] Available at: https://www.mathworks.com/help/releases/R2021a/documentation-center.html [Accessed: 06 June 2026]

[29] Low, B. K., Tang, S. K., Choa, V. J. "Arching in piled embankments", Journal of Geotechnical Engineering, 120(11), pp. 1917–1938, 1994. https://doi.org/10.1061/(ASCE)0733-9410(1994)120:11(1917)

[30] Russell, D., Pierpoint, N. "An assessment of design methods for piled embankments", Ground Engineering, 30(10), pp. 39–44, 1997.

[31] British Standards Institution "BS 8006-1:2010, Code of practice for strengthened/reinforced soils and other fills", BSI, London, 2010.

[32] German Geotechnical Society (ed.) "Recommendations for Design and Analysis of Earth Structures using Geosynthetic Reinforcements – EBGEO", Ernst & Sohn, Berlin, 2011. ISBN 978-3-433-02983-1. https://doi.org/10.1002/9783433600931

[33] Van Eekelen, S. J. M., Bezuijen, A., Van Tol, A. F. "Analysis and modification of the British Standard BS8006 for the design of piled embankments", Geotextiles and Geomembranes, 29(3), pp. 345–359, 2011 https://doi.org/10.1016/j.geotexmem.2011.02.001

[34] Carlson, B. O. "Armerad jord – beräkningsprinciper för banker på pålar" (Reinforced soil – calculation principles for embankments on piles), Terranova, Swedish Geotechnical Institute, Linköping, Sweden, 1987. (in Swedish)

[35] British Standards Institution "BS 8006:1995, Code of practice for strengthened/reinforced soils and other fills", BSI, London, 1995.

[36] Horgan, G. J., Sarsby, R. W. "The arching effect of soils over voids and piles incorporating geosynthetic reinforcement", In: Proceedings of the 7th International Conference on Geosynthetics, Nice, France, 2002, p. 523.

[37] Han, J., Gabr, M. A. "Numerical analysis of geosynthetic-reinforced and pile-supported earth platforms over soft soil", Journal of Geotechnical and Geoenvironmental Engineering, 128(1), pp. 44–53, 2002. https://doi.org/10.1061/(ASCE)1090-0241(2002)128:1(44)

[38] Nordic Geotechnical Society "Nordic handbook: reinforced soils and fills", Nordic Geotechnical Society, Stockholm, 2002.

[39] Jenck, O., Dias, D., Kastner, R. "Soft ground improvement by vertical rigid piles: two-dimensional physical modelling and comparison with current design methods", Soils and Foundations, 45(6), pp. 15–30, 2005. https://doi.org/10.3208/sandf.45.15

[40] Naughton, P. J. "The significance of critical height in the design of piled embankments", In: Soil Improvement, 2007, pp. 1–10. https://doi.org/10.1061/40916(235)3

[41] Chen, R. P., Xu, Z. Z., Chen, Y. M., Ling, D. S., Zhu, B. "Field tests on pile-supported embankments over soft ground", Journal of Geotechnical and Geoenvironmental Engineering, 136(6), pp. 777–785, 2010. https://doi.org/10.1061/(ASCE)GT.1943-5606.0000295

[42] Xu, C., Song, S., Han, J. "Scaled model tests on influence factors of full geosynthetic-reinforced pile-supported embankments", Geosynthetics International, 23(2), pp. 140–153, 2016. https://doi.org/10.1680/jgein.15.00038

[43] Van Eekelen, S. J. M., Brugman, M. H. A. (eds.) "Design guideline basal reinforced piled embankments – CUR 226", CRC Press, Boca Raton, 2016. https://doi.org/10.1201/9781315389806

[44] Filz, G. M., Sloan, J. A., McGuire, M. P., Smith, M., Collin, J. "Settlement and vertical load transfer in column-supported embankments", Journal of Geotechnical and Geoenvironmental Engineering, 145(10), 04019083, 2019. https://doi.org/10.1061/(ASCE)GT.1943-5606.0002130

[45] Lee, T., Van Eekelen, S. J., Jung, Y. H. "Numerical verification of the concentric arches model for geosynthetic-reinforced pile-supported embankments", Canadian Geotechnical Journal, 58(3), pp. 441–454, 2021. https://doi.org/10.1139/cgj-2019-0625

[46] Samira, F., Larbi, M., Mouloud, M., Laurent, B. "Subsoil compressibility effect in an end-bearing scaled pile-supported embankment", Innovative Infrastructure Solutions, 7(1), 75, 2022. https://doi.org/10.1007/s41062-021-00672-0

[47] Smith, E. J., Bouazza, A., King, L. E., Rowe, R. K. "New insights into soil arching behavior in column-supported embankments", Canadian Geotechnical Journal, 59(6), pp. 901–921, 2022. https://doi.org/10.1139/cgj-2021-0186

[48] Xu, Z., Zhang, L., Peng, B., Zhou, S. "DEM–FDM numerical investigation on load transfer mechanism of GESC-supported embankment", Computers and Geotechnics, 138, 104321, 2021. https://doi.org/10.1016/j.compgeo.2021.104321